Coupling of X-AES Transitions and XPS Photopeaks to Assess the Oxide Formation of Ga and in CuIn 0.7 Ga 0.3 Se 2 Material During Air Aging

Anna Gagliardi, Neal Fairley, Amelle Rebai, Arnaud Etcheberry, Negar Naghavi, Jean-françois Guillemoles, Muriel Bouttemy, Solène Béchu

Surface and Interface Analysis

WILEY

SURFACE and INTERFACE ANALYSIS

RESEARCH ARTICLE

Coupling of X-AES Transitions and XPS Photopeaks to Assess the Oxide Formation of Ga and in $CuIn_{0.7}Ga_{0.3}Se_2$ Material During Air Aging

Anna Gagliardi[1] | Neal Fairley[2] | Amelle Rebai[3] | Arnaud Etcheberry[1] | Negar Naghavi[3] | Jean-François Guillemoles[3] | Muriel Bouttemy[1] | Solène Béchu[1]

[1]Institut Lavoisier de Versailles (ILV), Université de Versailles Saint-Quentin-En-Yvelines, Université Paris-Saclay, CNRS, Versailles Cedex, France | [2]Casa Software Ltd, Devon, UK | [3]Institut Photovoltaïque d'Île-de-France (IPVF), UMR 9006, CNRS, Ecole Polytechnique – IP Paris, Chimie Paristech – PSL, Palaiseau, France

Correspondence: Solène Béchu (solene.bechu@uvsq.fr)

Received: 6 November 2024 | **Revised:** 22 January 2025 | **Accepted:** 27 January 2025

Funding: This work was supported by Agence Nationale de la Recherche (ANR-22-CE50-0008-01).

Keywords: CIGS aging | fixed depth profiling | photoemission spectroscopy | X-AES decomposition

ABSTRACT

The solar absorber Cu $(In_{0.7}Ga_{0.3})Se_2$ (CIGS) undergoes a process of evolution upon exposure to the atmosphere, resulting in the growth of oxide phases. This phenomenon can potentially affect the interfacial properties of CIGS, which in consequence may impact the efficiency of the solar cell. X-ray photoelectron spectroscopy (XPS) is an appropriate method to analyze the degradation of CIGS upon air aging. However, many photopeaks and Auger lines of the constitutive elements are distributed along the energy scale, and the exact determination of the degradation within the CIGS absorber requires specific care to select peaks to consider to ensure that information arise from similar escape depths. In this study, we propose to investigate the kinetics of degradation of Ga and In at similar depths probed by coupling not only photopeaks but also X-Auger electron spectroscopy (X-AES) transitions in the absence of photopeaks in the same energy range. If photopeaks modeling is well established for In and Ga, a decomposition procedure of the X-AES transitions must be developed. Both linear and nonlinear least square fitting were used and compared, starting to model CIGS, In_2O_3, and Ga_2O_3 references to deploy it after on Auger transitions measured on aged samples. Thanks to the determination of the degradation ratios (oxide phase over CIGS phase) at 3, 7, and 9 nm depth, we show that both In and Ga exhibit similar kinetic of oxide formation, which proceeds gradually by O penetration through the subsurface of the material, this penetration being more and more attenuated deeper.

1 | Introduction

In light of the prevailing climatic circumstances, it is imperative to intensify efforts towards the energy transition. Solar energy offers a number of advantages across a range of areas within the energy mix. The variety of solar cells and solar absorbers available, for instance, represents a significant benefit. Among the latter, $CuIn_xGa_{1-x}Se_2$ (CIGS) absorber stands out for its potential to modify its bandgap [1], to demonstrate intrinsic stability [2], to yield high efficiency [3], and to be coupled with other absorbers in the form of tandem cells [4].

While several developments have been made to increase yields from 19% in the 2000s to 23.6% today [3], the stability of cells has only recently become a subject of investigation, and few studies report on the absorber modifications itself. A number of

parameters have been identified as responsible for solar cell and absorber degradation, including temperature, relative humidity, and atmospheric pollutants [5, 6].

The monitoring of degradation products through nanometric or micrometric depths can be achieved by utilizing diverse characterization techniques. X-ray photoemission spectroscopy (XPS) is a highly effective technique for gaining insight into the chemical composition and evolution of chemical environments within the first nanometers of the CIGS absorber below the surface. Previous literature has demonstrated that aging-related changes in CIGS lead to the emergence of oxide phases [7, 8], and additionally, with different kinetics according to the element [9]. Indeed, elements III, which share the same crystallographic site (Figure 1) [10], tend to have faster oxide growths than elements I or VI during air aging.

This study aims to determine whether a discernible difference exists in the air reactivity of elements III within the CIGS network, using degradation ratios corresponding to different depths probed. As the evolution of elements I and VI was demonstrated in our preceding studies [7, 9], they will not be discussed here. This work could have been performed using angle-resolved photoemission recorded in a parallel mode [11]. However, intensities being lower for grazing angles, the recording time for this technique is quite lengthy, especially when high energy resolution is required to detect the first sign of degradation. In this study, we propose taking advantage of the selection of photopeaks at different kinetic energies (K.E.) to investigate different depths [9, 12, 13]. With an Al Kα excitation source, several photopeaks can be measured along the energy scale for In and Ga, as displayed in Figure 2. Among all these photopeaks, only Ga 3d and In 4d exhibit similar kinetic energies (1468.6 ± 0.1 eV and 1470.6 ± 0.1 eV, K.E., respectively) and thus a similar depth probed of approximately 9 nm. However, no comparative diagnosis of degradation is accessible at shallower depths, as no duet of photopeaks exists at lower kinetic energy.

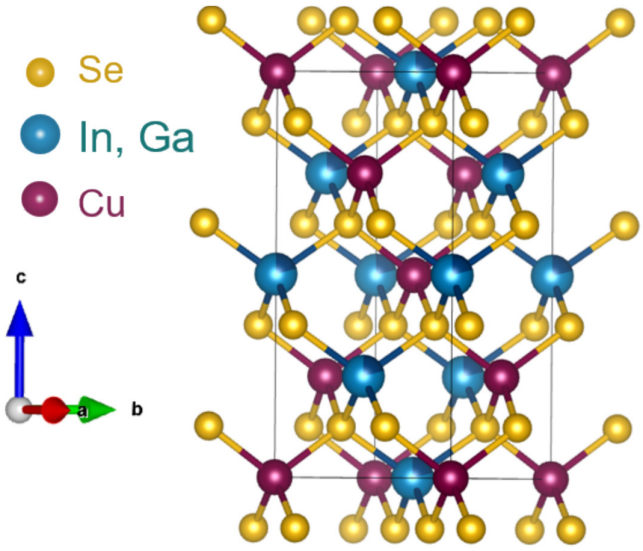

FIGURE 1 | Crystallographic structure of CIGS adapted from Souilah et al. [10].

To compensate for this lack, one potential solution is the utilization of X-Auger electron spectroscopy (X-AES) transitions situated nearby In 3d and Ga 2p photopeaks. The In $M_{4,5}N_{4,5}N_{4,5}$ line can be associated with the Ga 2p photopeak, thereby providing access to the deterioration of the extreme surface of the CIGS during aging till approximately 3 nm. Similarly, the Ga $L_3M_{4,5}M_{4,5}$ X-AES transition is situated just near the In 3d photopeak, informing about the chemistry till approximately 7 nm in this case.

To ascertain the chemical environments generated during the aging of the CIGS absorber, it is essential to decompose the X-AES line, as it is done for photopeaks. In the case of X-AES the decomposition process is not straightforward due to the complexity of the Auger transition shape. Two decomposition methods of X-AES transitions can be used, namely, the linear and the nonlinear decompositions [13]. The nonlinear decomposition is the most prevalent method employed in the processing of photoemission spectroscopy data [14]. When applied to X-AES transitions, this model requires the introduction of a significant number of arbitrary peaks, with potential adjustments in terms of their positions and full width at half maximum (FWHM) values. However, this procedure can lead to an extensive number of peaks, and thus potentially numerous decomposition errors. Conversely, the linear decomposition proceeds by implementing a defined chemical shape in the decomposition [15]. This method relies on a more challenging process (choice of the background, definition of the shape, and no possible adjustments), yet it may present fewer decomposition errors. The two decomposition methods will be employed here to determine the degradation ratio of In and Ga elements (i.e., the area ratio between the oxide contribution and the CIGS one) with the previously mentioned X-AES lines in comparison with In 3d and Ga 2p degradation ratios obtained after decomposition. This information at 3 and

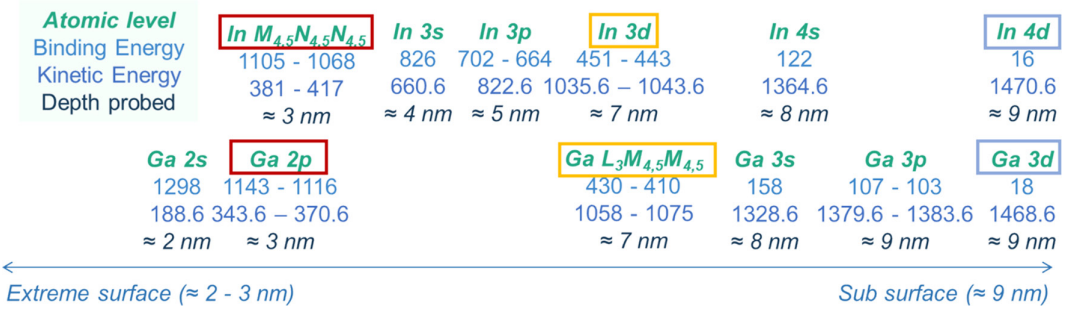

FIGURE 2 | Energetic distribution in binding and kinetic energies of the photopeaks and X-AES lines of Ga and In with an Al source.

7 nm will be completed with the values obtained with Ga 3d–In 4d photopeaks at 9 nm, bringing a clearer vision about the synergy or not of the In and Ga degradation mechanism during 1850 h aging in ambient air.

2 | Experimental Section

2.1 | Materials and Aging

Thick soda-lime glass with a thickness of 3 mm is coated with a layer of molybdenum presenting a thickness of 300 nm by direct current (DC) magnetron sputtering from a target comprising 99.95% pure molybdenum. Subsequently, a layer of CIGS measuring 500 nm is deposited on the surface using a single-step thermal evaporation process (approximately 500°C). This resulted in average ratios measured by X-ray fluorescence of 0.86 ± 0.02 for the CGI and 0.35 ± 0.02 for the GGI, without any gradient.

The In_2O_3 reference is obtained from a naturally aged metallic In ingot, and the Ga_2O_3 reference sources from Ga_2O_3 powder (Thermo Scientific, 99.99%).

The CIGS absorbers are subjected to an aging process in ambient air (20°C, with a relative humidity varying between 35 and 65%) for a total of 1850 h and are subsequently analyzed at 125, 250, 400, 550, 925, 1150, and 1850 h post-aging. Before the aging process, all potential oxides phases or side phases are removed with a chemical treatment of HCl 2 mol L^{-1} for 5 min followed by a KCN treatment (1 mol L^{-1} during 5 min).

2.2 | Surface Analysis and Data Treatment

The acquisition of XPS photopeaks and X-AES transitions is conducted on a Thermo Scientific Nexsa spectrometer equipped with a monochromatic Al Kα X-ray source (1486.6 eV). The spectrometer is calibrated in accordance with the Thermo Electron procedure, utilizing metallic Cu and Au samples as internal references (Cu $2p_{3/2}$ at 932.6 eV and Au $4f_{7/2}$ at 84.0 eV). Samples are grounded on the sample holder using a metallic pin-hole system. The experiments are conducted at a pressure range of 10^{-9} to 10^{-8} mbar. The high-energy resolution spectra are acquired using an X-ray spot size of 400 μm, a constant analyzer energy (CAE) mode of 20 eV, an energy step size of 0.1 eV, and a dwell time of 100 ms, resulting in an acquisition time of 2 h per CIGS sample. These parameters result in an energy resolution of 0.52 eV and a full width at half maximum (FWHM) value of 0.62 eV for the Ag $3d_{5/2}$ internal reference. The survey spectra (displayed in Figure S1) are recorded with a CAE of 200 eV and an energy step size of 1 eV. No charge neutralization is applied during these experiments, except for the measurement of Ga_2O_3 reference.

Data are processed with the CASAXPS software (version 2.3.25) [16], using the Al-Thermo-1 library. For all photopeaks and X-AES transitions, U2 Tougaard backgrounds are used. The convolution of Gaussian and Lorentzian functions is employed to describe the peak shape, with the ratio between the Gaussian and Lorentzian components varying according to the photopeak or X-AES transition in question. The specific ratio employed is LA(90) for Ga $2p_{3/2}$, LA(75) for In $3d_{5/2}$, Ga 3d, and In 4d, and LA(30) for X-AES combinations.

The calculated depth probed values are based on the inelastic mean free path (IMFP) values of the different transitions, which are determined using the QUASES-IMFP-TPP2M version 3.0 software with the nonrelativistic TPP-2 M formula for CIGS material and oxide phases (Ga_2O_3 and In_2O_3) [17]. These values are presented in Table 1, and the depth probed are calculated according to the formula:

$$Depth\ probed \approx 3 \times IMFP \quad (1)$$

3 | Results and Discussion

3.1 | Decomposition of Reference Samples Spectra

A comprehensive description of the evolution of In $M_{4,5}N_{4,5}N_{4,5}$ and Ga $L_3M_{4,5}M_{4,5}$ X-AES transitions over air aging necessitates the utilization of appropriate references to perform coherent decompositions. Literature reveals that, during aging in standard conditions, CIGS absorbers tend to form oxide phases and, more specifically, In_2O_3 and Ga_2O_3 [7–9, 18, 19]. It is therefore

TABLE 1 | IMFP values for the CIGS, Ga_2O_3, and In_2O_3 photopeaks and X-AES lines considered.

		Ga $2p_{3/2}$	Ga $L_3M_{4,5}M_{4,5}$	Ga 3d	In $3d_{5/2}$	In $M_4N_{4,5}N_{4,5}$	In 4d
CIGS	KE (eV)	369.0	1065.6	1467.0	1041.9	407.7	1468.8
	IFMP (nm)	1.099	2.365	3.029	2.324	1.175	3.032
	Depth probed (nm)	3.3	7.1	9.1	7.0	3.5	9.1
Ga_2O_3	KE (eV)	368.4	1062.4	1466.4			
	IFMP (nm)	0.884	1.865	2.387			
	Depth probed (nm)	2.7	5.6	7.2			
In_2O_3	KE (eV)				1041.6	405.4	1468.0
	IFMP (nm)				1.856	0.948	2.410
	Depth probed (nm)				5.6	2.8	7.2

Note: Kinetic energies are given with an error of 0.1 eV and depth probed with 0.2 nm.

anticipated that two distinct chemical environments for each element will be observed during the aging process, necessitating an initial decomposition step: the pristine CIGS and the oxide phases.

The In_2O_3 and CIGS In $M_{4,5}N_{4,5}N_{4,5}$ X-AES lines are displayed in Figure 3a. In this envelope, two Auger transitions are merged (In $M_4N_{4,5}N_{4,5}$ and In $M_5N_{4,5}N_{4,5}$). The In $M_4N_{4,5}N_{4,5}$ transitions are observed at 404.6 ± 0.1 and 407.7 ± 0.1 eV, K.E., for In_2O_3 and CIGS chemical environments, respectively. The In $M_5N_{4,5}N_{4,5}$ transitions emerge at 397.4 ± 0.1 and 400.2 ± 0.1 eV, K. E, respectively. Figure 3b displays the nonlinear (top) and the linear (bottom) decompositions for the global In $M_{4,5}N_{4,5}N_{4,5}$ X-AES line measured on CIGS. In regard to linear decomposition, the most challenging aspect is the delineation of the background and its boundaries. In this case, a unique U 2 Tougaard background is defined for the In $M_{4,5}N_{4,5}N_{4,5}$ X-AES transitions when monitoring air aging. The nonlinear decomposition (Figure 3b, top) is performed using arbitrary peaks constrained in position, FWHM and area [13], fixed in relation to the In $M_4N_{4,5}N_{4,5}$ transition peak positioned at 407.7 ± 0.1 eV, K.E. In total, nine peaks are required to fully describe the In $M_{4,5}N_{4,5}N_{4,5}$ CIGS X-AES line (Table 2). Similarly, linear and nonlinear decompositions are performed for In_2O_3 reference. Regarding the nonlinear decomposition (Figure 3c, top), six arbitrary peaks (Table 2) are necessary, the first one being positioned at the In $M_4N_{4,5}N_{4,5}$ line and the others referring to it. Although the decomposition is arbitrary, certain rules have been established for the FWHM values, which cannot exceed 10 eV. Furthermore, due to the initial arbitrary definition of the parameters used, this nonlinear decomposition presents one possibility and may differ from others presented in the literature [20].

The Ga $L_3M_{4,5}M_{4,5}$ X-AES lines of Ga_2O_3 and CIGS (Figure 4a), wherein the predominant transitions are noticed at 1062.1 ± 0.1 eV and 1065.3 ± 0.1 eV, K.E., respectively, are modeled using the same procedures. For the nonlinear decomposition of CIGS Ga $L_3M_{4,5}M_{4,5}$ X-AES transition (Figure 4b, top), four supplementary arbitrary peaks have been fixed in regard to the principal peak, which is positioned at 1065.3 ± 0.1 eV (Table 3). The Ga $L_3M_{4,5}M_{4,5}$ line of Ga_2O_3, Figure 4c (top), is also constituted of five arbitrary peaks that are described in Table 3. The CIGS and Ga_2O_3 linear decompositions (Figure 4b, top) proceed as for the In $M_{4,5}N_{4,5}N_{4,5}$ X-AES lines, by the positioning of the background which remains fix.

To ensure that the CIGS X-AES lines are free from any traces of oxide chemical environments, it is essential to also decompose

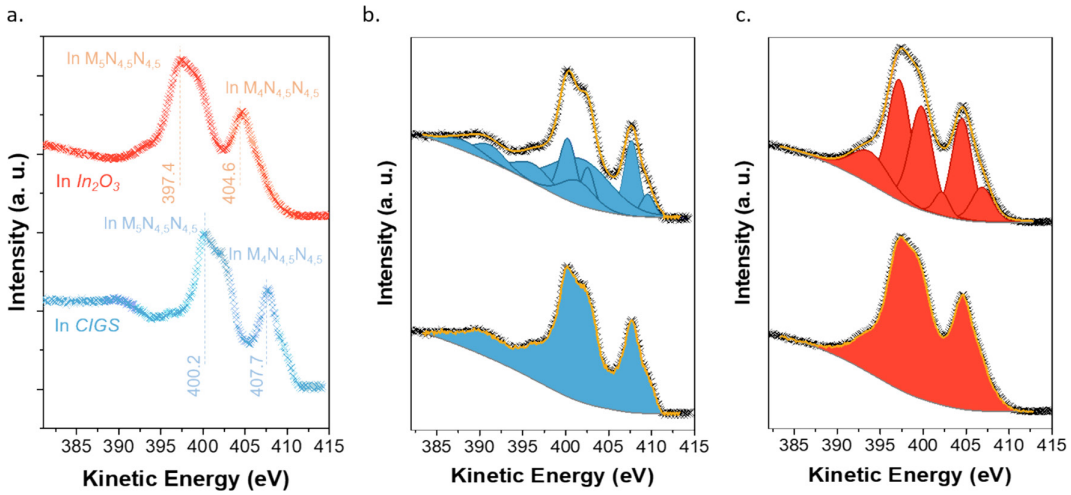

FIGURE 3 | In $M_{4,5}N_{4,5}N_{4,5}$ X-AES lines for In_2O_3 and CIGS. (a) Nonlinear (top) and linear (bottom) least-square decompositions of In $M_{4,5}N_{4,5}N_{4,5}$ X-AES lines of CIGS (b) and In_2O_3 (c).

TABLE 2 | In $M_{4,5}N_{4,5}N_{4,5}$ arbitrary decomposition parameters for CIGS and In_2O_3 environments (positions are provided in kinetic energy).

		Principal peak (PP)	Peak 2	Peak 3	Peak 4	Peak 5	Peak 6	Peak 7	Peak 8	Peak 9
CIGS	Position (eV)	407.7 ± 0.1	PP + 1.8	PP − 5.1	PP − 5.8	PP − 6.3	PP − 7.4	PP − 11.5	PP − 16.5	PP − 19.5
	FWHM (eV)	2.10 ± 0.05	PP*0.87	PP*0.87	PP*3.91	PP*2.14	PP*1.11	PP*2.34	PP*2.04	PP*2.45
	Area	—	PP*0.26	PP*0.46	PP*2.41	PP*0.67	PP*0.91	PP*0.59	PP*0.46	PP*0.34
In_2O_3	Position (eV)	404.5 ± 0.1	PP + 2.4	PP − 2.3	PP − 4.7	PP − 7.3	PP − 10.7			
	FWHM (eV)	2.85 ± 0.05	PP*1.02	PP*0.71	PP*1.11	PP*1.13	PP*1.81			
	Area	—	PP*0.35	PP*0.17	PP*1.13	PP*1.34	PP*0.58			

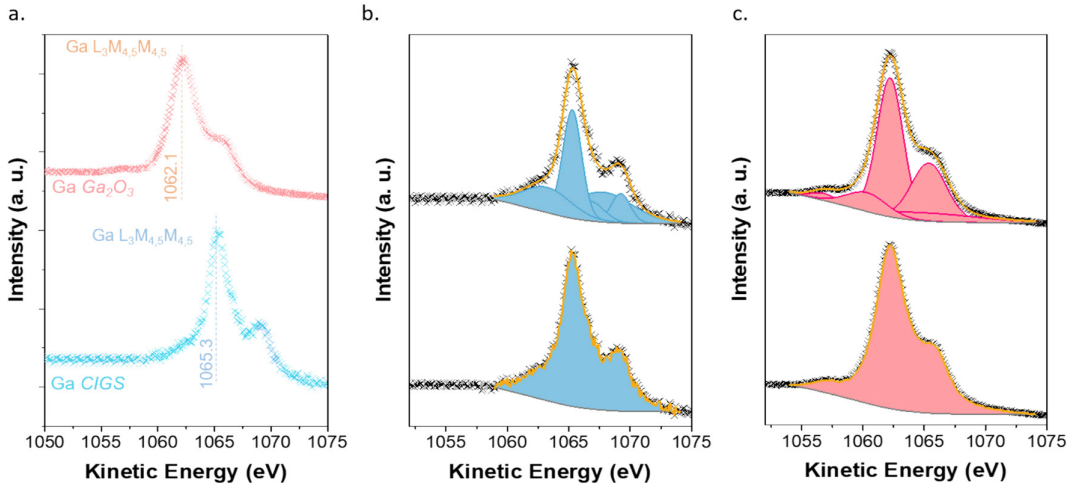

FIGURE 4 | Ga $L_3M_{4,5}M_{4,5}$ X-AES lines for Ga_2O_3 and CIGS. (a) Nonlinear (top) and linear (bottom) least-square decompositions of Ga $L_3M_{4,5}M_{4,5}$ X-AES lines of CIGS (b) and Ga_2O_3 (c).

TABLE 3 | Ga $L_3M_{4,5}M_{4,5}$ arbitrary decomposition parameters for CIGS and Ga_2O_3 environments (positions are provided in kinetic energy).

		Principal peak (PP)	Peak 2	Peak 3	Peak 4	Peak 5
CIGS	Position (eV)	1065.3 ± 0.1	PP − 2.0	PP + 1.47	PP + 2.5	PP + 4.0
	FWHM (eV)	1.85 ± 0.05	PP*2.57	PP*1.46	PP*3.15	PP*0.99
	Area	—	PP*0.60	PP*0.27	PP*0.87	PP*0.27
Ga_2O_3	Position (eV)	1062.2 ± 0.1	PP − 1.9	PP − 5.4	PP + 3.1	PP + 3.2
	FWHM (eV)	2.52 ± 0.05	PP*1.57	PP*0.98	PP*1.36	PP*3.85
	Area	—	PP*0.21	PP*0.05	PP*0.57	PP*0.23

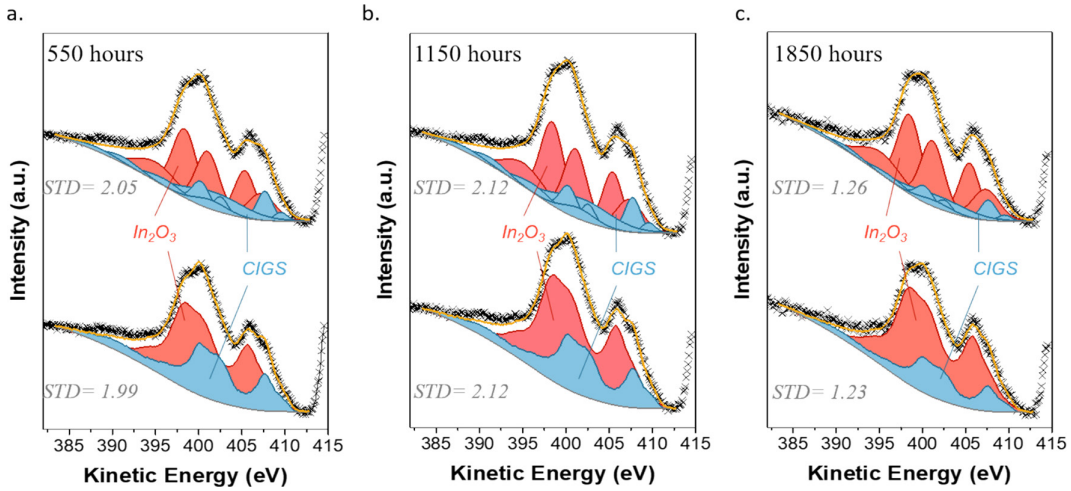

FIGURE 5 | In $M_{4,5}N_{4,5}N_{4,5}$ X-AES lines evolution after 550 h (a), 1150 h (b), and 1850 h (c) of aging. Nonlinear and linear least square decompositions are top and bottom spectra, respectively. The residual standard deviations (STD) are indicated for each decomposition.

the corresponding peaks (i.e., Ga 2p, Ga 3d, In 3d, and In 4d) and to compare them with the O 1s photopeak. For all of the photopeaks constituent of CIGS, solely the CIGS contribution is noticed (Figure S2 and Table S1), as described in the literature [7, 9]. The O 1s photopeak is typical of a surface contamination photopeak (531.8 ± 0.1 eV, Table S1).

3.2 | Applications to CIGS Aging Study

The oxide formation over air aging of In and Ga is apprehended using the linear and nonlinear fitting procedure of In $M_{4,5}N_{4,5}N_{4,5}$ and Ga $L_3M_{4,5}M_{4,5}$ X-AES lines to determine the proportion of pristine CIGS and oxide phases using the

procedures established for the references. Prior to any aging process (i.e., at t = 0 h), photopeaks examination confirms that only the CIGS chemical environment is detected. The decomposition of the In $M_{4,5}N_{4,5}N_{4,5}$ X-AES line (Figure S3) proceeds then by using solely the fit of the CIGS reference, whether for the linear or nonlinear decomposition. Once the aging process has started, the addition of the oxide environment is essential for achieving a satisfactory decomposition of the In $M_{4,5}N_{4,5}N_{4,5}$ X-AES lines. As illustrated in Figure 5, the In_2O_3 chemical environment increases over time and becomes predominant after 550 h of aging (Figure 5a). Between 550 and 1150 h of aging (Figure 5b), the In_2O_3 chemical environment content remains relatively stable. Remarkably, after 1850 h of aging (Figure 5c), there is a noticeable increase in the amount of oxide phase. Once starting aging, a Na 1 s photopeak, which was not present on the pristine surface, is discernible and positioned at 417.5 eV ± 0.1 eV, KE. This photopeak is very close in term of energy with the In $M_{4,5}N_{4,5}N_{4,5}$ X-AES spectra but not overlapping with it. This phenomenon is well known and inherent to the migration over time of sodium from the soda-lime substrate through the absorber [21–24].

The residual standard deviation analysis reveals that comparable decomposition qualities are attained when contrasting the nonlinear and the linear decompositions. With regard to the evolution of the degradation ratio, slight differences are observed when using one decomposition or the other (see Table 4). However, given that the relative errors are less than 10%, this discrepancy remains acceptable between the two methods, especially when it is used in a comparative way.

As for In, the evolution of the Ga $L_3M_{4,5}M_{4,5}$ X-AES transition over air aging is satisfactorily modeled using CIGS chemical environment and Ga_2O_3 oxide phase [18]. Again, prior to any aging step (i.e., at t_0), we can state with the help of photopeaks that a sole CIGS chemical environment is sufficient to accurately describe the Ga $L_3M_{4,5}M_{4,5}$ X-AES line (Figure S4). On Figure 6, the nonlinear and the linear decompositions of the Ga $L_3M_{4,5}M_{4,5}$ X-AES line are provided for 550 h (Figure 6a), 1150 h (Figure 6b), and 1850 h of aging (Figure 6c). After 550 h of air aging (Figure 6a), the oxide contribution is clearly visible but not predominant yet. It keeps increasing with aging time (Figure 6b), and becomes predominant after 1850 h (Figure 6c). In regard to the comparison of linear and nonlinear decompositions, a good coherence between both is obtained, whether looking at the residual standard deviation (Figure 6) or the relative error obtained from the degradation ratio (Table 4).

The discrepancy in the observed relative error between the decompositions of the In $M_{4,5}N_{4,5}N_{4,5}$ and Ga $L_3M_{4,5}M_{4,5}$ X-AES lines can be primarily attributed to greater latitude on fitting parameters for the nonlinear decomposition. The impact of the

TABLE 4 | Evolution of the atomic ratio of the oxide chemical environment over the CIGS chemical environment for linear and nonlinear decomposition for In $M_{4,5}N_{4,5}N_{4,5}$ and Ga $L_3M_{4,5}M_{4,5}$ X-AES lines.

Aging time (h)			0	125	250	400	550	925	1150	1850
In $M_{4,5}N_{4,5}N_{4,5}$	$\frac{\%\,at.(In_2O_3)}{\%\,at.(CIGS)}$	Linear	0.00	0.62	0.94	1.25	1.68	1.91	1.97	2.80
		Nonlinear	0.00	0.60	0.91	1.16	1.71	1.79	1.91	2.81
	Relative error (%)		/	3.7	2.4	6.6	1.7	6.4	3.1	0.5
Ga $L_3M_{4,5}M_{4,5}$	$\frac{\%\,at.(Ga_2O_3)}{\%\,at.(CIGS)}$	Linear	0.00	0.38	0.52	0.64	0.73	0.84	0.84	1.13
		Nonlinear	0.00	0.39	0.54	0.65	0.75	0.53	0.86	1.15
	Relative error		/	1.5	4.0	2.1	2.5	2.0	1.6	1.2

Note: The atomic ratios are given with an error of 0.05. Relative errors are provided in percentage.

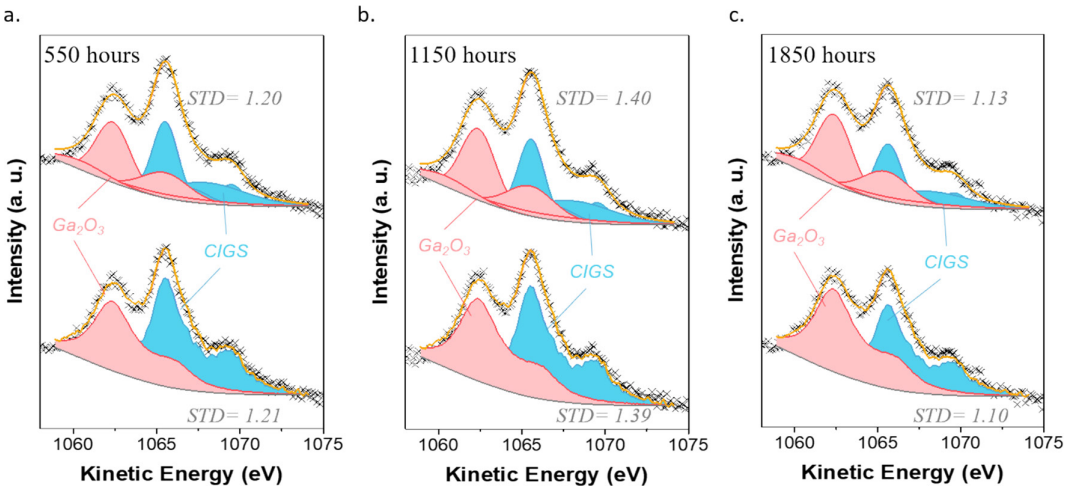

FIGURE 6 | Ga $L_3M_{4,5}M_{4,5}$ X-AES lines evolution after 550 h (a), 1150 h (b), and 1850 h (c) of aging. Nonlinear and linear least square decompositions are top and bottom spectra, respectively. The residual standard deviations (STD) are indicated for each decomposition.

flexibility of the principal peaks (in terms of both position and FWHM value) will be greater for a decomposition with a total of 15 peaks (In $M_{4,5}N_{4,5}N_{4,5}$) than for a decomposition with a total of 10 peaks (Ga $L_3M_{4,5}M_{4,5}$). Therefore, it can be stated that nonlinear and linear decompositions may differ more when the number of peaks in the nonlinear decomposition is higher.

3.3 | CIGS Oxide Formation at Different Depth Probed

To unveil if a difference is noticeable between the reactivity of Ga and In within the network of CIGS, different degradation ratios are calculated using the previously mentioned pairs of photopeaks/X-AES transitions (Figure 2, Ga $2p_{3/2}$/In $M_{4,5}N_{4,5}N_{4,5}$, ≈ 3 nm; In $3d_{5/2}$/Ga $L_3M_{4,5}M_{4,5}$, ≈ 7 nm; and Ga 3d/In 4d, ≈ 9 nm).

Figure 7a illustrates the decomposition of the Ga $2p_{3/2}$ photopeak. Starting with the same surface state as the one of the CIGS reference sample prior to aging, only the CIGS chemical environment at 1117.8 ± 0.1 eV, B.E. is needed, while the Ga_2O_3 contribution at 1118.2 ± 0.1 eV, B.E. has to be added after 1850 h of aging. Similarly, a single CIGS chemical environment (444.8 ± 0.1 eV, B.E.) is required for In $3d_{5/2}$ photopeak at the initial aging stage. However, the In_2O_3 environment (445.1 ± 0.1 eV, B.E.) becomes necessary to complete the description of the 1850-h aging spectrum (Figure 7b). The decomposition of the Ga 3d/In 4d photopeaks is more complex due to the superimposition of the doublet peaks of Ga 3d and the In 4d (Figure 7c). The full decomposition procedure is presented elsewhere [25]. If at t_0 only the CIGS chemical environment is required for the Ga 3d In 4d region decomposition (In $4d_{5/2}$ at 17.9 ± 0.1 eV, B.E. and Ga $3d_{5/2}$ at 19.7 ± 0.1 eV, B.E.), it becomes necessary to add oxide environments for In and Ga for 1850 h of aging (In $4d_{5/2}$ at 18.7 ± 0.1 eV, B.E. and Ga $3d_{5/2}$ at 20.2 ± 0.1 eV, B.E.). One can note that after aging, all photopeaks presented in Figure 7 show an intensity decrease, due to carbon contamination. Although it is not possible to assess it with the C 1 s photopeak, due to its overlap with the Se $L_2M_{4,5}M_{4,5}$ X-AES transition, the C $KL_{2,3}L_{2,3}$ transition (Figure S5) shows a substantial modification over air aging.

The same decompositions are applied to all the photopeaks acquired over aging time to calculate degradation ratios which are displayed, as well as the ratios obtained with the X-AES transitions decompositions, in Figure 7d. As soon as the aging starts, the data are divided into three different series according to the associated depths probed. The Ga 3d and In 4d photopeaks which present a higher escape depth, that is, probing deeper from the surface, show a lower kinetic of oxide formation rate. On the contrary, the oxide formation rate of the Ga $2p_{3/2}$ photopeak and the In $M_{4,5}N_{4,5}N_{4,5}$ X-AES transition, which have the lowest escape depth, raises faster than the others.

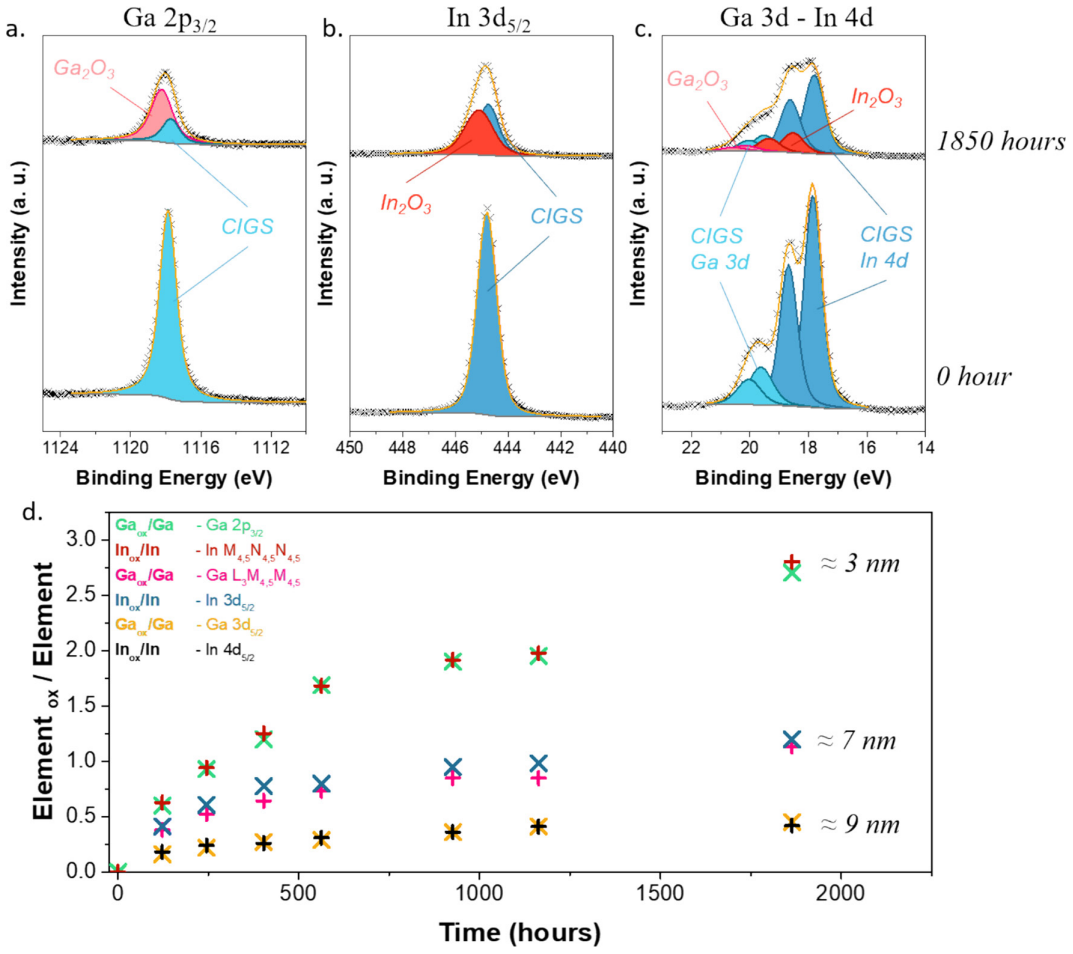

FIGURE 7 | Curves fitted to the data of Ga $2p_{3/2}$ (a), In $3d_{5/2}$ (b) and the Ga 3d–In 4d region (c) before aging (bottom spectra) and after 1850 h of aging (top spectra). Evolution of the degradation ratio over time for different photopeaks and X-AES transitions (d).

Interestingly, both In and Ga follow the same trend at the three probed depths. After 125 h of aging, oxide phases are observed at all depths probed. However, the quantity of oxide phase is significantly greater at the extreme surface, indicating that although oxygen incorporation occurs gradually over time, this process is not uniform. This hypothesis is confirmed when prolonging aging until 925 h, the increase of oxide quantity being more pronounced at the extreme surface than at 7 or 9 nm, evidencing a slowdown of oxygen incorporation within the CIGS absorber.

4 | Conclusions

To investigate the kinetic reactivity of elements III in CIGS material during air aging, we propose an innovative approach that couples chemical assessments using XPS photopeaks and X-AES transitions with similar escape depths. While XPS photopeak decomposition is well documented, especially for Ga and In in CIGS material, the decomposition of the X-AES line is more challenging and requires to develop specific decomposition procedures. In this work, we present two different approaches, the linear least square decomposition and the nonlinear least square decomposition, having pros and cons with regard to their implementation way and flexibility. In examining the evolution of the CIGS surface upon air aging, by comparing the degradation ratios, we observed a progressive correlated oxide formation for Ga and In, with a progressive penetration of O into the material network. In and Ga exhibit similar kinetics of oxide formation over air aging, which is in good agreement with the fact that they share the same crystallographic site. The coupling of XPS photopeaks and X-AES transitions to get information at comparable probed depth is implementable to other materials in place of more time-consuming analysis methods, such as AR XPS, HAXPES, or depth profiling.

Acknowledgements

This work has been carried out in the frame of the ADECS project (ANR-22-CE50-0008-01) supported by the "Agence Nationale de la Recherche."

Data Availability Statement

The data that support the findings of this study are available from the corresponding author upon reasonable request.

References

1. M. Contreras, J. Tuttle, D. Du, et al., "Graded Band-Gap $Cu(In,Ga)Se_2$ Thin-Film Solar Cell Absorber With Enhanced Open-Circuit Voltage," *Applied Physics Letters* 63 (1993): 1824–1826.

2. J. F. Guillemoles, "Stability of $Cu(In,Ga)Se_2$ Solar Cells: A Thermodynamic Approach," *Thin Solid Films* 361–362 (2000): 338–345.

3. NREL, "Best Research-Cell NREL Efficiency Chart," can be found under https://www.nrel.gov/pv/cell-efficiency.html, **2024**.

4. T. J. Jacobsson, A. Hultqvist, S. Svanström, et al., "2-Terminal CIGS-Perovskite Tandem Cells: A Layer by Layer Exploration," *Solar Energy* 207 (2020): 270–288.

5. M. Theelen and F. Daume, "Stability of $Cu(In,Ga)Se_2$ Solar Cells: A Literature Review," *Solar Energy* 133 (2016): 586–627.

6. A. Debono, N. Fikree, A. Julien, et al., "Impact of Agricultural Atmospheric Pollutants on the Opto-Electrical Performance of CIGS Solar Cells," *Progress in Photovoltaics: Research and Applications* 32 (2024): 814–826.

7. A. Loubat, S. Béchu, M. Bouttemy, et al., "Cu Depletion on $Cu(In,Ga)Se_2$ Surfaces Investigated by Chemical Engineering: An X-Ray Photoelectron Spectroscopy Approach," *Journal of Vacuum Science and Technology A* 37 (2019): 041201.

8. W. Calvet, B. Ümsür, A. Steigert, et al., "In Situinvestigation of as Grown $Cu(In,Ga)Se_2$ Thin Films by Means of Photoemission Spectroscopy," *Journal of Vacuum Science and Technology A* 37 (2019): 031510.

9. S. Béchu, M. Bouttemy, J. Guillemoles, and A. Etcheberry, "The Influence of Relative Humidity Upon $Cu(In,Ga)Se_2$ thin-Film Surface Chemistry: An X-Ray Photoelectron Spectroscopy Study," *Applied Surface Science* 576 (2022): 151898.

10. M. Souilah, A. Lafond, C. Guillot-Deudon, S. Harel, and M. Evain, "Structural Investigation of the Cu_2Se–In_2Se_3–Ga_2Se_3 Phase Diagram, X-Ray Photoemission and Optical Properties of the $Cu_1-z(In_{0.5}Ga_{0.5})1+z/3Se_2$ Compounds," *Journal of Solid State Chemistry* 183 (2010): 2274–2280.

11. M. S. Vinodh and L. P. H. Jeurgens, "Quantitative Analysis of Angle-Resolved XPS Spectra Recorded in Parallel Data Acquisition Mode," *Surface and Interface Analysis* 36 (2004): 1629–1636.

12. M. Wortmann, K. Viertel, M. Westphal, et al., "Sub-Nanometer Depth Profiling of Native Metal Oxide Layers Within Single Fixed-Angle X-Ray Photoelectron Spectra," *Small Methods* 8, no. 3 (2024): 2300944.

13. S. Béchu and N. Fairley, "Determination of the X-Auger Electron Spectroscopy Evolution of Indium in InSb by Linear and Nonlinear Least Squares Approaches," *Journal of Vacuum Science and Technology A* 42 (2024): 013202.

14. J. J. Moré, "Numerical Analysis, chapter The Levenberg-Marquardt Algorithm. Implementation and Theory," *Lecture Notes in Mathematics* 630 (1978): 105–116.

15. G. H. Golub and C. Reinsch, "Singular Value Decomposition and Least Squares Solutions," *Numerische Mathematik* 14 (1970): 403–420.

16. N. Fairley, V. Fernandez, M. Richard-Plouet, et al., "Systematic and Collaborative Approach to Problem Solving Using X-ray Photoelectron Spectroscopy," *Applied Surface Science Advances* 5 (2021): 100112.

17. S. Tanuma, C. J. Powell, and D. R. Penn, "Calculations of Electron Inelastic Mean Free Paths. V. Data for 14 Organic Compounds Over the 50–2000 eV Range," *Surface and Interface Analysis* 21 (1994): 165–176.

18. J. Lehmann, S. Lehmann, I. Lauermann, et al., "Reliable Wet-Chemical Cleaning of Natively Oxidized High-Efficiency $Cu(In,Ga)Se_2$ Thin-Film Solar Cell Absorbers," *Journal of Applied Physics* 116 (2014): 233502.

19. D. Hauschild, F. Meyer, S. Pohlner, et al., "Impact of Environmental Conditions on the Chemical Surface Properties of $Cu(In,Ga)(S,Se)_2$ Thin-Film Solar Cell Absorbers," *Journal of Applied Physics* 115 (2014): 183707.

20. J. D. Henderson, L. Pearson, H. Nie, and M. C. Biesinger, "X-Ray Photoelectron Spectroscopy Analysis of Indium and Indium-Containing Compounds," *Surface and Interface Analysis* 57 (2025): 81–97.

21. M. Theelen, V. Hans, N. Barreau, H. Steijvers, Z. Vroon, and M. Zeman, "The Impact of Alkali Elements on the Degradation of CIGS Solar Cells," *Progress in Photovoltaics: Research and Applications* 23 (2015): 537–545.

22. D. Shin, J. Kim, T. Gershon, et al., "Effects of the Incorporation of Alkali Elements on $Cu(In,Ga)Se_2$ Thin Film Solar Cells," *Solar Energy Materials & Solar Cells* 157 (2016): 695–702.

23. O. Nwakanma, S. Velumani, and A. Morales-Acevedo, "Review on the Effects due to Alkali Metals on Copper–Indium–Gallium–Selenide Solar Cells," *Materials Today Energy* 20 (2021): 100617, https://doi.org/10.1016/j.mtener.2020.100617.

24. C. K. Boumenou, H. Phirke, J. Rommelfangen, et al., "Nanoscale Surface Analysis Reveals Origins of Enhanced Interface Passivation in RbF Post Deposition Treated CIGSe Solar Cells," *Advanced Functional Materials* 33, no. 30 (2023): 2300590.

25. S. Béchu, A. Loubat, M. Bouttemy, J. Vigneron, J.-L. Gentner, and A. Etcheberry, "A Challenge for X-Ray Photoelectron Spectroscopy Characterization of Cu(In,Ga)Se_2 absorbers: The Accurate Quantification of Ga/(Ga + In) Ratio," *Thin Solid Films* 669 (2019): 425–429.

Supporting Information

Additional supporting information can be found online in the Supporting Information section.